Journal of Thermal Analysis and Calorimetry, Vol. 89 (2007) 2, 427–440

THERMAL DECOMPOSITION MECHANISMS COMMON TO POLYURETHANE, EPOXY, POLY(DIALLYL PHTHALATE), POLYCARBONATE AND POLY(PHENYLENE SULFIDE)

K. L. Erickson[*]

Sandia National Laboratories [1], P.O. Box 5800, Albuquerque, NM 87185, USA

Thermal decomposition of polyurethane, epoxy, poly(diallyl phthalate), polycarbonate, and poly(phenylene sulfide) was examined using a combination of thermal and chemical analysis techniques. Thermal gravimetric analysis with simultaneous analysis of evolved gases by Fourier transform infrared spectroscopy, differential scanning calorimetry, and gas chromatography coupled with Fourier transform infrared spectroscopy were used to obtain rate data, determine enthalpy changes, and identify decomposition products. Examination of the evolved decomposition products indicated a common set of chain scission mechanisms involving the aromatic moieties in each of the polymer materials studied.

Keywords: *decomposition, epoxy, polycarbonate, poly(diallyl phthalate), poly(phenylene sulphide), polyurethane*

Introduction

Thermal decomposition of organic polymers is important in many scientific and engineering applications. Thermal decomposition of polymers has been studied from a scientific perspective to gain insight into molecular structure, and from an engineering perspective to determine how specific materials behave at elevated temperatures. A particular area of interest is the behavior of polymer materials in fire environments.

Organic polymer materials are used frequently in structures and transportation systems. In an oxidizing environment, polymer materials can provide the fuel that propagates a fire. In a non-oxidizing environment, polymer materials can be damaged catastrophically as a result of an incident heat flux. Modeling the response of such structures and systems in fire environments has important applications in safety and vulnerability analyses. In either oxidizing or non-oxidizing environments, the thermal decomposition chemistry of the organic polymer materials often is an important factor. Specific applications include predicting the flux of volatile species to a flame region, predicting the extent of thermally induced mechanical damage in structural composite materials, predicting pressure growth in closed containers, modeling liquefaction and flow of decomposing materials, particularly foams, determining the toxicity of evolved gases and vapors, and characterizing char formation.

The role of polymer decomposition in fire dynamics was discussed by Drysdale [2]. Other general references pertinent to fire and polymers include Babrauskas and Grayson [3] and Nelson and Wilkie [4, 5]. Applications of polymer decomposition in systems safety analyses involving polymer materials in an inert environment were discussed by Erickson *et al.* [6], Sun *et al.* [7] and Hobbs *et al.* [8, 9]. Results from investigations, prior to 1964, of thermal decomposition of polymers were well described by Madorsky [10]. Results from later investigations, but prior to 2000, of thermal decomposition of polymers were summarized by Raave [11]. Earlier investigations, particularly those discussed by Madorsky were done without the benefit of modern thermal analysis equipment and techniques, which are now widely used to study the thermal stability, degradation, and decomposition of polymer materials. General discussions of modern thermal analysis equipment and techniques were given by Haines [12], Sorai [13] and Šesták [14]. Application of these techniques to develop rate expressions for fire dynamics modeling were discussed by Nicolette *et al.* [15] and Vembe *et al.* [16].

In recent investigations thermal analysis (TA) particularly thermogravimetry (TG) as well as derivative thermogravimetry (DTG) and calorimetry especially differential scanning calorimetry (DSC) have been used either separately or in combination to study thermal decomposition of numerous materials. These include flame retardant polycarbonate [17], conducting polyanilines [18], wood treated with

* klerick@sandia.gov

1388–6150/$20.00

Akadémiai Kiadó, Budapest, Hungary
Springer, Dordrecht, The Netherlands

flame retardants [19], jute/vinyl ester composites [20], poly(vinyl chloride) plasticized with polyesterurethane [21], carbonaceous materials used as diesel soot surrogates [22], semi-interpenetrating polymer networks of polyurethane and poly(vinyl chloride) [23], poly(ether-ketone/sulfone) imides and poly(ether-ketone/sulfone) ethylimide [24], cellulose-hyphan and its complexes with some transition and indium metal ions [25], poly(2,2'-dimethoxy-4,4'-biphenylenevinylene) [26], epoxy-smectite nanocomposites [27], polystyrene synthesized in the presence of carbomethyl cellulose [28], polyisobutylene and isobutylene-isoprene copolymers [29], silicone caoutchouc polymers and silicone rubbers [30], aromatic polyamides with benzimidazolyl side group [31], rice husk flour filled polypropylene and high-density polyethylene composites [32], non-filled and filled porous copolymers of divinylbenzene with styrene or some acrylic monomers [33], epoxy-diamine systems subjected to alternative curring cycles [34, 35], vinylidene chloride/vinyl chloride copolymers in the presence of N-substituted maleimides [36] and acrylic ion-exchange resins [37].

Many of the preceding authors developed rate expressions to represent their experimental TG and DSC results. Frequently, those expressions were of the form

$$d\alpha/dt = K(T)f(\alpha)$$

where $K(T)=A\exp(-Q/RT)$; A is a constant (frequency factor); Q is the activation energy; R is the gas constant; T is absolute temperature; t is time, and α is the degree of conversion for the thermal decomposition process ($0\leq\alpha\leq1$). An excellent overview of the various approaches is given by Šesták [14]. Specific applications are discussed by Polli *et al.* [38], Criado *et al.* [39, 40], Rychlý *et al.* [41], Budrugeac and Segal [42], and Schneider and Bíró [43]. Some of the authors suggested chemical mechanisms based on the functional form of $f(\alpha)$. Work reported by Li and Koseki [44] and Gröbler and Kada [45] included discussions of methods for inferring decomposition mechanisms from thermal analysis data and the functional form of $f(\alpha)$. However, since thermal decomposition of polymers can involve complicated chemical and physical processes, several authors have questioned the validity of mechanisms inferred from only thermal analysis data. Informative critiques have been provided by Galwey [46], Howell [47, 48], Vyazovkin [49], Brown [50] and Šimon [51, 52]. Additionally, the effects of nucleation were discussed by Ozawa [53]; the issues of bubble formation and migration were discussed by Kojima *et al.* [54] and the influence of heating rate was discussed by Bigda [55] and Shlensky *et al*. [56, 57].

In some applications, it is desirable to develop rate expressions in terms of the mechanisms controlling formation of low molecular mass decomposition products and the molecular mass distribution of the degraded polymers. Examples of such applications include systems safety analyses involving multiple thermal decomposition mechanisms that control pressure growth in closed containers [6], as well as liquefaction and flow of degraded polymer materials [7]. Determining decomposition mechanisms generally requires use of combined thermal and chemical analysis techniques. In general, the application of combined techniques has been more limited than the use of thermal analysis alone. Rybiński *et al.* [58] used thermal analysis and oxygen index to examine thermal stability and flammability of butadiene-acrylonitrile rubber cross-linked with iodoform. Chruściel *et al.* [59] similarly used thermal analysis, oxygen index, and FTIR to examine thermal stability and flammability of butadiene-acrylonitrile rubber modified in bulk and on a surface by poly(methylsiloxanes). Howell *et al*. [60] used thermal and spectroscopic techniques to study the degradation of vinylidene chloride/[4-(*t*-butoxycarbonyloxy)phenyl]methyl acrylate copolymers.

The use of evolved gas analysis (EGA) in conjunction with thermal analysis, particularly TG, can provide substantial insight into decomposition mechanisms. However, condensed-phase processes are inferred from the observed gas and vapor species. Sinfrônio *et al.* [61] used TG combined with mass spectrometry (MS) to investigate the thermal degradation and catalytic decomposition of high-density polyethylene over solid acid catalysts. Pappa *et al.* [62] also used combined TG-MS to investigate effects of fire retardants on the pyrolysis of pine-needles and their components. Pielichowski [63] and Pielichowski and Stoch [64] used TG-FTIR and DSC to study, respectively, thermal degradation poly(vinyl chloride)/polyaniline conducting blends and polystyrene brominated on the ring.

When multiple decomposition products evolve from a sample, the spectra obtained with TG-MS and TG-FTIR are the superposition of the spectra from each of the decomposition products. Often the identification of individual species is difficult. In some cases, the use of pyrolysis coupled with GC-MS has been used to identify decomposition products. Cascaval *et al.* [65] used TG and pyrolysis-GC to examine degradation of polymers of ethylene glycol dimethacrylate. Xie and Pan [66] used TG-FTIR, TG-MS, and pyrolysis/GC-MS for thermal characterization of organically modified clays, polymers, and coal blends. Also, Xie *et al.* [67] used TG-FTIR, TG-MS, and pyrolysis/GC-MS to examine the

thermal degradation of polyimides. A new EGA-MS instrument reported by Tsugoshi [68] was based on a skimmer interface and ion attachment mass spectrometry and detected species that were not detected previously by pyrolysis/GC-MS.

Since the use of combined thermal and chemical analysis techniques has been much less common than the use of thermal analysis alone, knowledge of decomposition mechanisms and reliable data for developing rate expressions are often lacking for materials of interest. To provide input to numerical models for systems safety analyses, thermal decomposition of several polymer materials have been experimentally investigated using multiple complementary experimental techniques to determine major decomposition mechanisms and to obtain rate date for developing rate expressions based on proposed decomposition mechanisms. Experiments have been organized to investigate mechanisms associated with the functional groups in different polymers.

Thermal gravimetric analysis and simultaneous analysis of evolved gases by Fourier transform infrared spectroscopy (FTIR) were used to obtain data for developing rate expressions and identifying decomposition products evolving from the sample. Differential scanning calorimetry was used to examine enthalpy changes during decomposition and to obtain additional insight into decomposition mechanisms. An additional technique involving thermal decomposition combined with GC-FTIR was used to obtain more detailed analysis of decomposition products. When feasible, infrared microprobe (IRMP) was used for postmortem analysis of condensed-phase residues.

The work described below is part of an ongoing effort to use a common set of thermal and chemical analysis techniques to develop a library of decomposition mechanisms and kinetics based on the chemical functional groups occurring in a variety of polymers. The experimental techniques are described first and are most closely related to the techniques used by Xie and Pan [66] and Xie *et al.* [67] referenced above. Then, results from thermal decomposition experiments are given for two polyurethanes (foams), an epoxy, a poly(diallyl phthalate) (DAP), a polycarbonate (PC), and a poly(phenylene sulfide) (PPS). The synthesis details of some of the materials studied are proprietary. One polyurethane formulation (TDI RPU) is based on toluene diisocyanate (TDI) and polyhydroxy polyesters derived from adipic acid. The other polyurethane formulation (MDI RPU) is based on methylene-4,4'diphenyl diisocyanate (MDI) and polyhydroxy polyethers. The epoxy material is made from EPON 828^{TM} (diglycidyl ether of bisphenol A) and Epikure^{TM} 3251 (aliphatic amine). The poly(diallyl phthalate) (DAP), polycarbonate (PC), and poly(phenylene sulphide) (PPS) were commercial products. Results for the TDI-based polyurethane are given first. The results are discussed in detail to illustrate the experimental approach. Furthermore, the TDI RPU provides an excellent example of reversible and competing reactions occurring during thermal decomposition. Results for the other materials are then summarized, and decomposition mechanisms are discussed.

Experimental

Much of the experimental data for thermal decomposition was obtained using TG-FTIR as shown schematically in Fig. 1a. A complementary technique based on GC-FTIR is shown schematically in Fig. 1b.

In Fig. 1a, the furnace purge gas exhaust of the TGA (TA Instruments Model 2950) was usually connected by a heated stainless steel transfer line to the TGA interface module of the FTIR spectrometer (Nicolet Magna 750). The purge gas was UHP N_2 flowing at 50 to 60 mL min^{-1}. The transfer line temperature was maintained at 300°C. The TG-FTIR

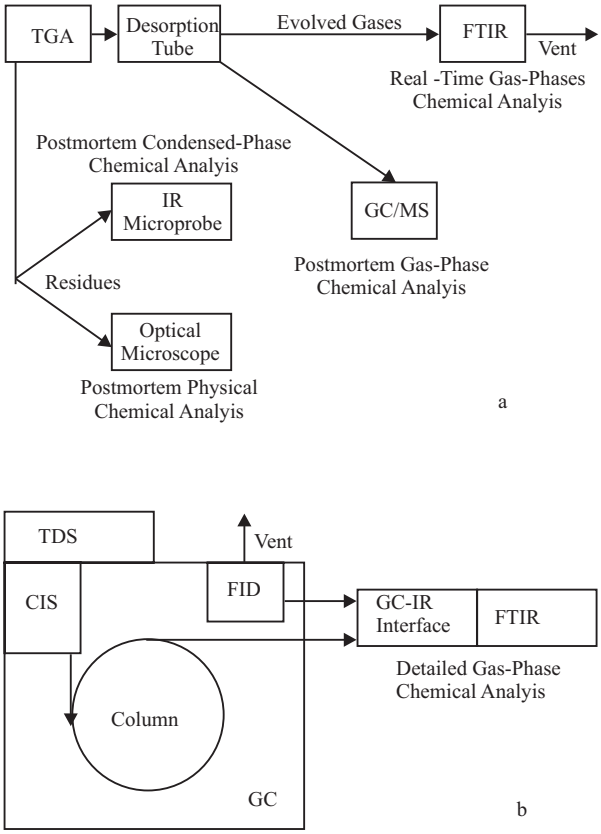

Fig. 1 Schematic diagram of TG-FTIR analysis and complementary methods: a – TG-FTIR and b – TDS-GC-FTIR

interface module in the auxiliary experiment compartment of the FTIR spectrometer was also maintained at 300°C. The FTIR spectrometer provided concurrent chemical analysis of the evolved gases. Multiple spectra were collected and averaged over consecutive 30 s intervals to provide average spectra as a function of time. The spectra acquired represented the superposition of the spectra from all of the gas phase constituents. When multiple species contributed overlapping signals, the interpretation of spectra and identification of decomposition products was difficult.

To obtain more detailed gas phase analyses, two techniques were used to complement the TG-FTIR experiments. The first technique is illustrated schematically in Fig. 1a. Desorption tubes, instead of the transfer line, were connected to the furnace purge gas outlet of the TG. Samples were collected at predetermined time intervals. The decomposition products deposited on the desorption tubes were subsequently analyzed by GC-MS.

The second technique is illustrated schematically in Fig. 1b. A thermal desorption system (TDS), a Gerstel TDS 4, was used as a small, temperature-programmable tube furnace. Samples were placed in an aluminum boat that was placed in an empty desorption tube in the TDS. As the sample was heated, the decomposition products were removed by the carrier gas, UHP He, and were quenched and retained in the cryogenic injection system (CIS), a Gerstel CIS 2. After sample heating was complete, the CIS was rapidly heated (12°C s^{-1}), and the decomposition products were injected onto the capillary column of the gas chromatograph. The carrier gas was monitored by the GC-IR interface module, and FTIR spectra were collected similarly to those collected in the TG-FTIR experiments. However, spectra were averaged over shorter, 3 to 6 s, time intervals. From the GC-IR interface, the carrier gas flowed through the flame ionization detector (FID) and was then vented.

The TG-FTIR experiments were done with small, about 2.5 to 5 mg, samples that were heated in unconfined and partially-confined sample pan configurations. The unconfined configuration consisted of samples in open, shallow 10 mm diameter platinum pans. The unconfined configuration was used to examine initial decomposition mechanisms under conditions that minimized effects of mass transfer and reversible and secondary reactions. The partially-confined configuration consisted of samples in sealed hermetic aluminum pans (TA Instruments) having lids with 60 μm circular orifices. The partially-confined configuration was used to examine effects of reversible, competing, or secondary reactions that would result from limiting mass transfer of decomposition products away from the sample. With one exception, the materials studied were ground into powders, which provided better reproducibility between replicate experiments. The exception was TDI RPU foam, which was not easily made into a powder. In this case, unconfined samples were thin discs. Partially-confined samples were small cylinders.

The DSC experiments also were done with small, about 2.5 to 5 mg, samples that were heated in unconfined and partially-confined sample pan configurations. In this case, the unconfined configuration involved open aluminum pans. The DSC used was a TA instruments model 2920. The purge gas was UHP N_2. The flow rate was about 60 mL min^{-1}.

When feasible, residues from the TG and DSC experiments were examined with the infrared microprobe (IRMP), as well as with an optical microscope. Since the residues usually contained multiple products, identification of specific products was difficult. However, the determination of functional groups in the residues was useful. FTIR spectra were usually obtained using attenuated total reflectance (ATR) with a diamond objective. Brittle residues were often difficult to analyze.

Results and discussion

Typical TG results from unconfined samples of the materials studied are shown in Fig. 2. The samples were heated at a constant rate of 20°C min^{-1}. The temperature range over which mass evolves from a sample will change slightly with heating rate. Increasing the heating rate shifts the plot of mass *vs.* temperature to slightly higher temperatures. This shift occurs because at higher heating rates, the sample is at each temperature for shorter time intervals than at lower heating rates, and less mass evolves at each temperature. Thus, as heating rate increases, the mass *vs.* temperature plot shifts toward higher temperatures. The shift is relatively small because the rate of reaction generally increases rapidly with temperature. The effect of heating rate is discussed in detail by Shlensky *et al.* [56, 57].

TDI-based rigid polyurethane foam

Figure 3a shows replicate TG results from samples of TDI RPU foam that were heated at a constant rate of 20°C min^{-1}. Results for both unconfined and partially-confined (60 μm orifice) samples are shown. The unconfined samples were thin discs weighing about 4 mg. The partially-confined configuration required smaller samples, about 2.5 mg cylinders.

Relative to the unconfined samples, the TGA response of the partially-confined samples is shifted

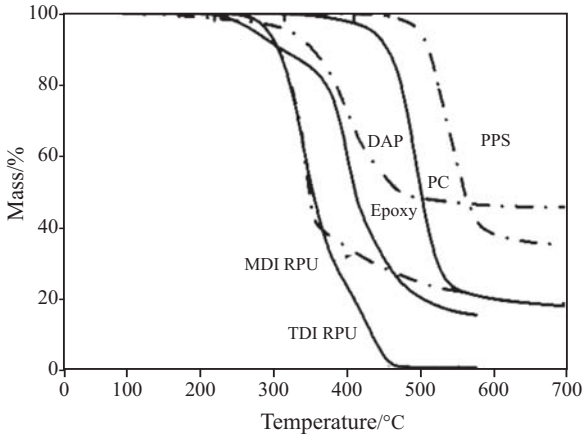

Fig. 2 Typical TG results from polymers heated at 20°C min^{-1} with UHP N_2 purge

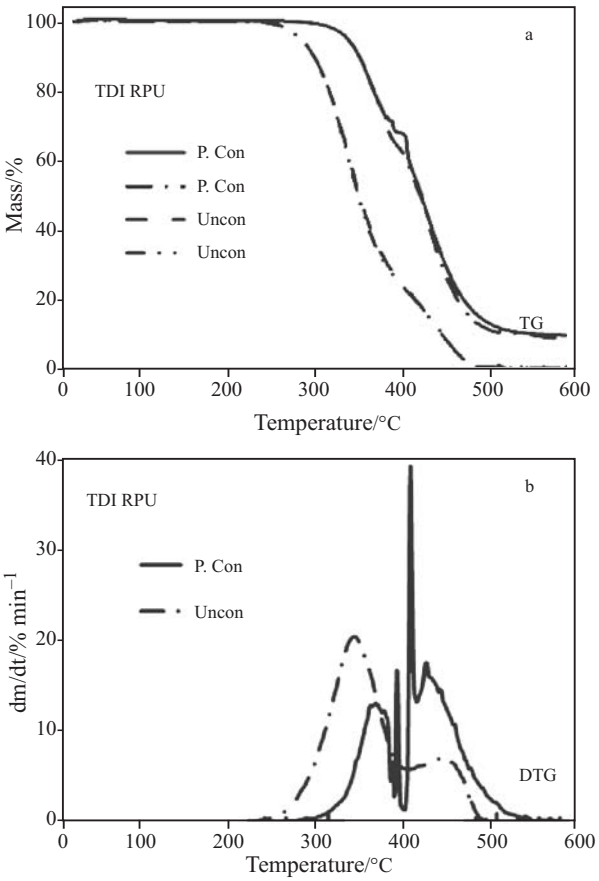

Fig. 3 Typical a – TG and b – DTG results for unconfined and partially-confined (60 μm orifice) samples of TDI RPU foam

significantly to higher temperatures. Some of this shift could be due to slower evaporation of decomposition products, but other processes are evident. In Fig. 3a, about 10% of the partially-confined sample formed a residue that decomposed very slowly at temperatures to about 1000°C. In Fig. 3b, the derivative (rate of mass loss) curve for the partially-confined sample is significantly different from the curve for the unconfined sample. This indicates that the dominant decomposition reactions may differ between unconfined and partially-confined samples. During the partially-confined experiments, the TDI RPU liquefied and flowed due to gas and vapor generation. The sharp oscillation in Fig. 3b resulted from the orifice temporarily plugging due to flow.

Additional insight into thermal decomposition process, as well as data for enthalpy changes, was obtained from DSC experiments, which were done with 4 mg unconfined samples and 2.5 mg partially-confined samples heated at 20°C min^{-1}. Typical data for unconfined and partially-confined (60 μm orifice) DSC samples are shown as a function of temperature in Figs 4a and b, respectively. In each figure, the endotherm is positive-valued, and the DSC data are compared with the corresponding TG derivative curves.

Comparing the TG and DSC results involves some uncertainty since the data were obtained from separate instruments. Nevertheless, in Fig. 4a, the net heat flow to the unconfined sample is entirely endothermic, primarily sensible heat, heat of decomposition reaction(s), and heat of vaporization.

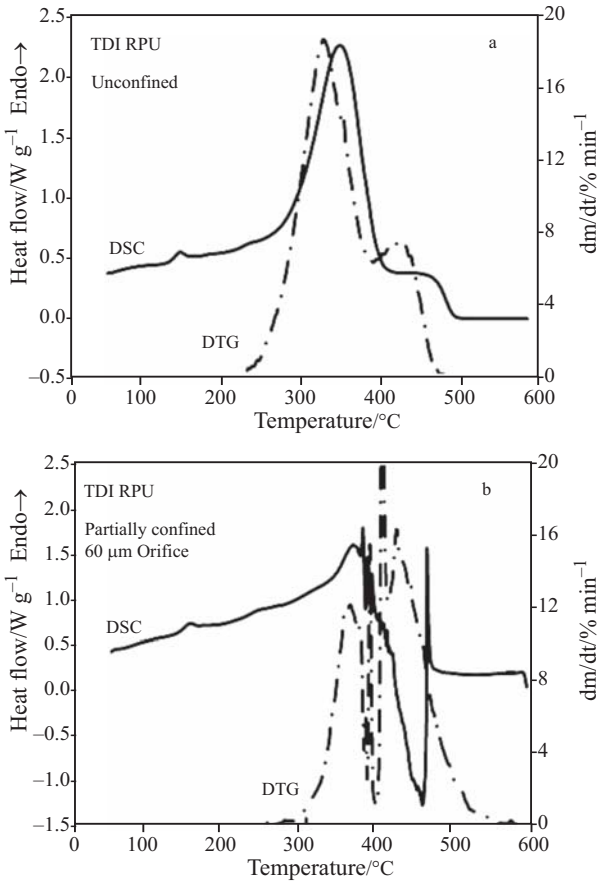

Fig. 4 Typical DSC and DTG results for TDI RPU compared with DTG curves: a – unconfined samples and b – partially-confined (60 μm orifice) samples

Furthermore, the heat flow closely follows the rate of mass loss from the TG sample. This indicates that decomposition of the sample is controlled by endothermic processes, and that the energy absorbed is proportional to the rate at which mass evolves from the sample. In Fig. 4b, the situation is much different. The net heat flow to the partially-confined sample is initially endothermic, to a temperature of about 350°C, and also follows the rate of mass loss from the sample. However, at temperatures between about 350 and 450°C, the heat flow to the sample dramatically decreases and becomes exothermic before becoming endothermic again at temperatures above 450°C.

The sharp decrease in heat flow occurs over the same temperature range in which the rate of mass loss is greatest. This is consistent with a change in the decomposition reactions that dominate as the sample is most rapidly decomposing. This effect could be due to a competing primary decomposition reaction proceeding relatively more rapidly as a result of partial confinement, or the effect could be due to primary decomposition products undergoing secondary reactions to form more thermally stable and (or) less volatile secondary products. Again, the sharp oscillations in Fig. 4b resulted from the orifice temporarily plugging as a result of liquefaction and flow.

The FTIR spectra that were collected during the TG experiments provide insight into the different mechanisms of thermal decomposition. Figure 5 shows the Gramm-Schmidt reconstruction (GSR) from the FTIR spectra that were collected during consecutive 30 s time intervals during the TG experiments shown in Fig. 3. For comparison, the rate of mass loss curves from the TG results shown in Fig. 3 are shown as a function of time in Fig. 5. The GSR is the integral of the FTIR signal intensity with respect to wavelength over an entire spectrum (about 4000–400 cm^{-1}). The IR signal intensity is a function of the concentrations of the IR absorbing species in the purge gas from the TG. The concentrations of species in the purge gas are proportional to their rate of evolution from the sample in the TG. In many cases, the GSR and the rate of mass loss curve will each have pronounced maxima. If those maxima occur at approximately the same time, as in Fig. 5, the spectra collected during the TG experiment are assumed to correspond closely in time with the TG results.

Figure 6 shows two spectra that were collected during a TG experiment (Figs 2 and 3) with an unconfined sample of TDI RPU. The spectrum in Fig. 6a was collected at 16.913 min, which corresponds to about 337°C in the TG experiment, and the rate of mass loss in Fig. 3b is approaching a maximum. A spectral library search using Nicolet

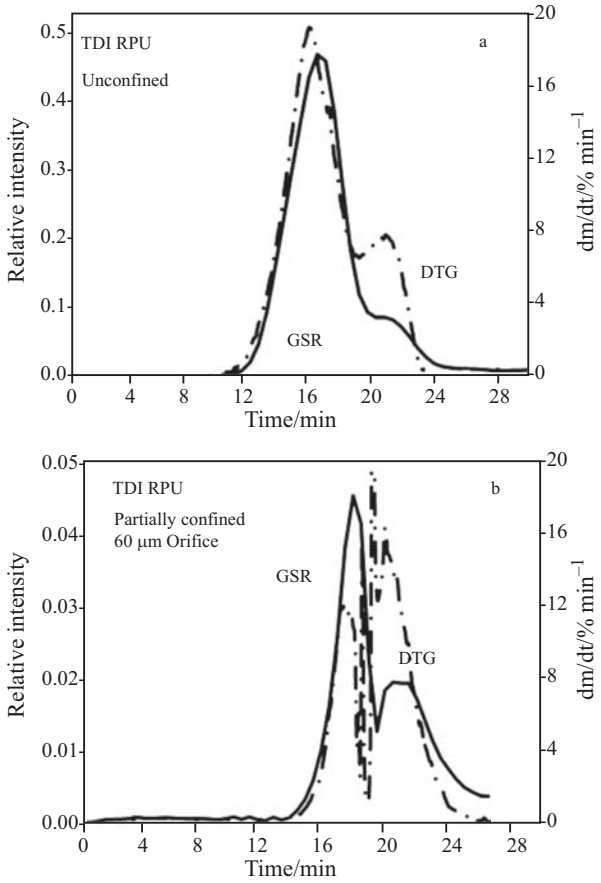

Fig. 5 Gramm-Schmidt reconstruction (GSR) for TDI RPU samples: a – unconfined and b – partially-confined

OMNIC software [69] showed that the spectrum matched the spectrum from a TDI standard provided by the manufacturer. The spectrum in Fig. 6b was collected at 21.038 min, which corresponds to about 420°C in the TG experiment, and the rate of mass loss is near the second, smaller maximum in Fig. 3b. The spectrum indicates the presence of TDI at much lower intensity, as well as additional products. The signal for carbon dioxide overlaps the left side of the TDI signal at about 2270 cm^{-1}. The signal at about 1750 cm^{-1} indicates the presence of a carbonyl compound and appears to correspond to cyclopentanone. The weaker signals between 1300 and 900 cm^{-1} indicate products containing C–O–C bonds. Evolution of TDI and cyclopentanone was confirmed by TG experiments in which decomposition products were collected on desorption tubes and analyzed by desorption into a GC–MS system.

FTIR spectra also were collected during the TG experiments (Fig. 3) with partially-confined samples. Figure 7 shows spectra collected at 16.917 and 21.978 min. The spectrum collected at 16.917 min (Fig. 7a) corresponds to about 341°C in Fig. 3. The spectrum collected at 21.978 min (Fig. 7b) corres-

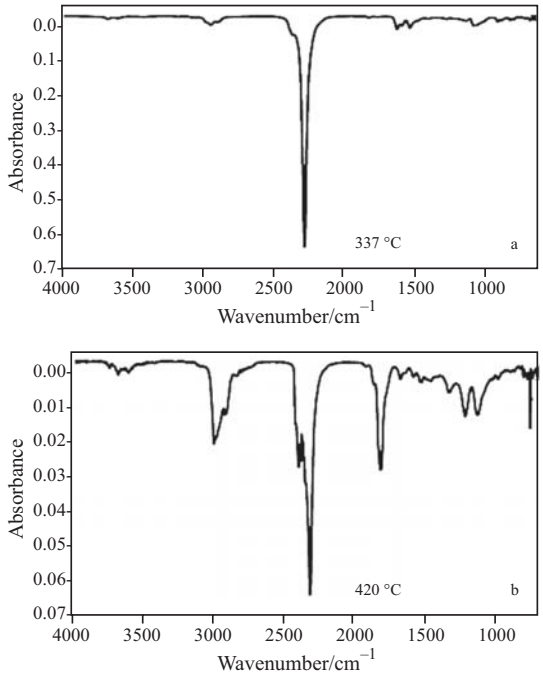

Fig. 6 Unconfined TDI RPU: FTIR spectra corresponding to GSR at a – 16.913 and b – 21.038 min

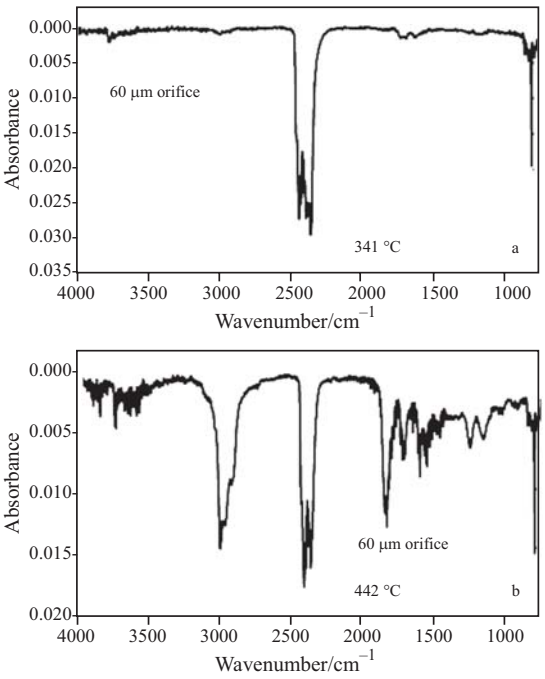

Fig. 7 Partially-confined TDI RPU: FTIR spectra corresponding to GSR at a – 16.917 and b – 21.978 min

ponds to about 442°C. Although the range on the absorbance scale differs significantly between Figs 6 and 7, important differences are evident in the spectra. The spectrum at 16.917 min shown in Fig. 7a and the spectrum at 16.913 min shown in Fig. 6a correspond to about the same temperature for the partially-confined and unconfined samples, respectively. However, in Fig. 7a, the TDI signal in the spectrum is greatly reduced relative to the carbon dioxide signal, when compared with the spectrum at 16.913 min shown in Fig. 6a. Furthermore, the spectrum at 21.978 min shown in Fig. 7b and the spectrum at 21.038 min shown in Fig. 6b also correspond to about the same temperature. The spectra in Figs 7b and 6b are similar, except for the small signals at about 1600 and 1500 cm^{-1} in Fig. 7b that could indicate the presence of an amine moiety in the decomposition products. The formation of toluene diamine was confirmed by additional TG experiments in which decomposition products were collected on desorption tubes and then analyzed by desorption into a GC–MS system.

Figure 8 shows results from a TDS-GC-FTIR experiment (Fig. 1b) with an unconfined sample of TDI RPU. During the first stage of the experiment, a 1 mg sample was heated at 20°C min^{-1} to 330°C and quenched. The GC-FTIR results identified TDI as the only major decomposition product. During the second stage (Fig. 8), the sample was heated at 20°C min^{-1} to 380°C, held at 380°C for 15 min, and then quenched. The GSR from the second-stage GC-FTIR analysis is shown in Fig. 8a. The time shown begins with the start of CIS heating. The spectrum from the large peak at 7.73 min is shown in Fig. 8b. The spectrum matches that for cyclopentanone, which appears to

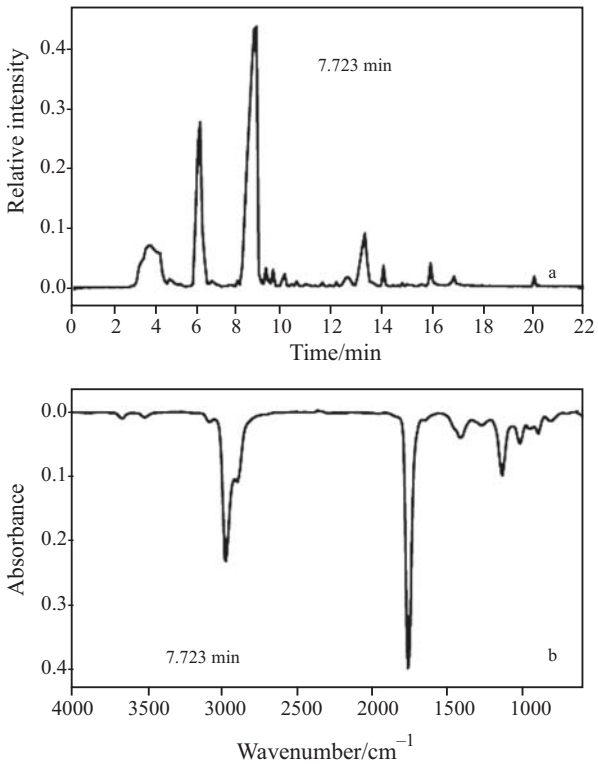

Fig. 8 Results from a TDS-GC-FTIR experiment with TDI RPU: a – GSR and b – sample spectrum

evolve from the adipate moiety in the polyhydroxy polyester. The large peak at 5.399 min is 2-ethyl-acrolein. The broad peak between 2 and 4 min appears to be a mixture of water, carbon dioxide and formaldehyde. Some water appears to be due to water contamination in the helium carrier. However, the major portion of the water appears to be formed during decomposition.

Based on the above results, decomposition of TDI RPU appears to be controlled by reactions involving the urethane functional group and scission of carbon-oxygen bonds in the polyhydroxy polyester moieties in the polymer. Reactions involving the urethane moiety are considered below. Reactions involving the polyhydroxy polyester moieties are deferred to a later paper.

Figure 9 shows a set of reactions involving the urethane moiety that appear consistent with the experimental data. Initially, the urethane linkage appears to cleave to reform the TDI and hydroxyl moieties. This reaction is reversible. If the TDI does not escape to the vapor phase, competing reactions result in evolution of carbon dioxide and formation of an amine moiety in the polymer, which subsequently evolves as toluene diamine.

The sequence of reactions forming toluene diamine is not certain. Most carbon dioxide associated with scission in the urethane groups appears to evolve from the partially-confined samples at temperatures between 280 and 380°C, which corresponds to the first peak in the derivative curve in Fig. 3b. In that temperature range, toluene diamine should readily evaporate and evolve with the carbon dioxide. Most toluene diamine evolves at higher temperatures, and postmortem IRMP analysis of residues indicates the presence of an amine moiety. This is consistent with formation of a polyamine as

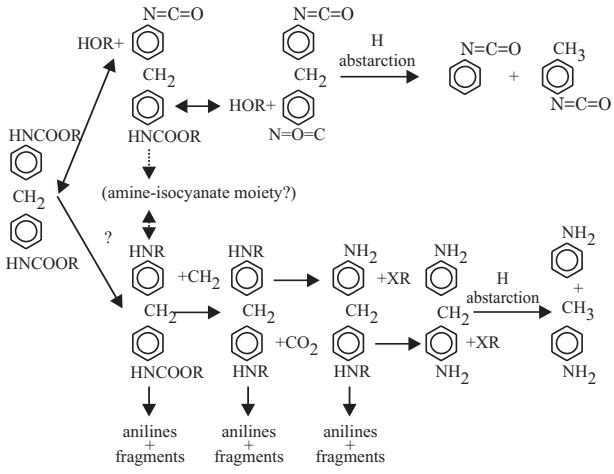

Fig. 9 TDI RPU decomposition reactions involving the urethane moiety in the polymer

carbon dioxide evolves. The polyamine then decomposes to form toluene diamine, which could also form directly from urethane moieties. The formation of carbodiimides and carbon dioxide is also possible, but no evidence for the reaction has been found. Finally, formation of an amino-isocyanate moiety, indicated in Fig. 9, should be possible, but no evidence of its formation has been found.

MDI-based rigid polyurethane foam

The initial stage of thermal decomposition of unconfined samples of MDI RPU and TDI RPU appear similar. At about 250°C, the sample mass begins to decrease noticeably. At temperatures between 300 and 350°C, the mass of the sample decreases rapidly to about 40% of the mass of the original sample. Above 350°C, the sample mass decreases more slowly. However, the rate at which the sample mass decreases at temperatures above 350°C differs significantly between the TDI RPU and MDI RPU samples. Between 350 and 500°C, the MDI RPU evolves mass at significantly diminished rates relative to TDI RPU. Above 500°C, the rate of mass loss of the MDI RPU is very slow to temperatures of about 1000°C. Results from partially-confined TG experiments with MDI RPU exhibit shifts with temperature. However, the shifts, particularly during the first half of decomposition are not as large as the shifts that occur with the TDI RPU [70].

Results from DSC experiments with unconfined samples of MDI RPU indicated that decomposition of MDI RPU is initially controlled by endothermic processes. However, at temperatures between about 300 and 350°C, decomposition of MDI RPU involves an exothermic process when the sample is most rapidly decomposing, which is similar to the results observed with partially-confined TDI RPU samples. Results from DSC experiments with partially-confined samples of MDI RPU also indicated an initial endothermic process that was followed by an exothermic process at temperatures between about 300 and 350°C. The exothermic response in the partially-confined samples was greater than in the unconfined samples [70].

The FTIR spectra obtained during the TG experiments with unconfined and partially-confined samples of MDI RPU were analogous to the spectra collected from samples of TDI RPU. Spectra from unconfined samples indicated evolution of isocyanates (probably phenyl isocyanates) and CO_2. However, the isocyanate signal was decreased relative to the isocyanate signal in the spectra from TDI RPU, and the CO_2 signal was significantly increased relative to the isocyanate signal. Spectra from partially-confined samples indicated a greatly

diminished isocyanate signal, a relatively increased CO_2 signal, and signals indicating amine moieties [70].

The TDS-GC-FTIR experiments with MDI RPU were done similarly to experiments with TDI RPU. Spectra from the first stage of heating indicated phenyl isocyanates. However, a library search did not provide conclusive identification. Spectra from the second stage of heating indicated that aniline and 4-methyl aniline were major decomposition products. Figure 10a shows the GSR from a TDS-GC-FTIR experiment with MDI RPU. The FTIR spectrum from the large peak at 11.282 min is shown in Fig. 10b. The spectrum matches that of aniline [69]. The spectrum corresponding to the prominent peak at 12.597 min matches that of 4-methylaniline [69]. The broad peak between 2 and 5 min appears to be water and ammonia [69]. Several of the smaller peaks appear to correspond to decomposition products from the polyhydroxy polyethers. The decomposition of which is deferred to a later paper.

Similar reactions involving the urethane moiety appear to control decomposition of both TDI RPU and MDI RPU. Decomposition of MDI RPU appears to be more complicated than decomposition of TDI RPU. Evolution of an isocyante moiety during the unconfined TG experiments indicates that urethane linkages cleave to reform the isocyanate and hydroxyl moieties. However, the MDI is less volatile than TDI,

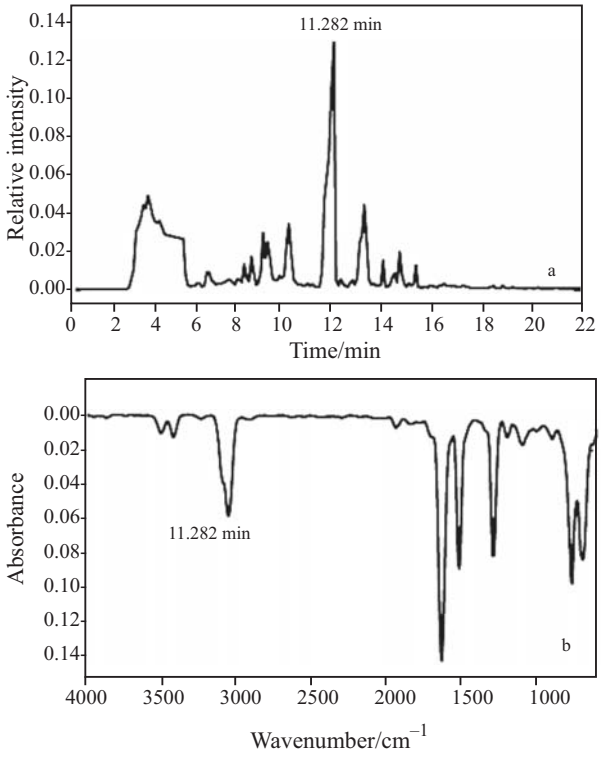

Fig. 10 Results from a TDS-GC-FTIR experiment with MDI RPU: a – GSR and b – sample spectrum

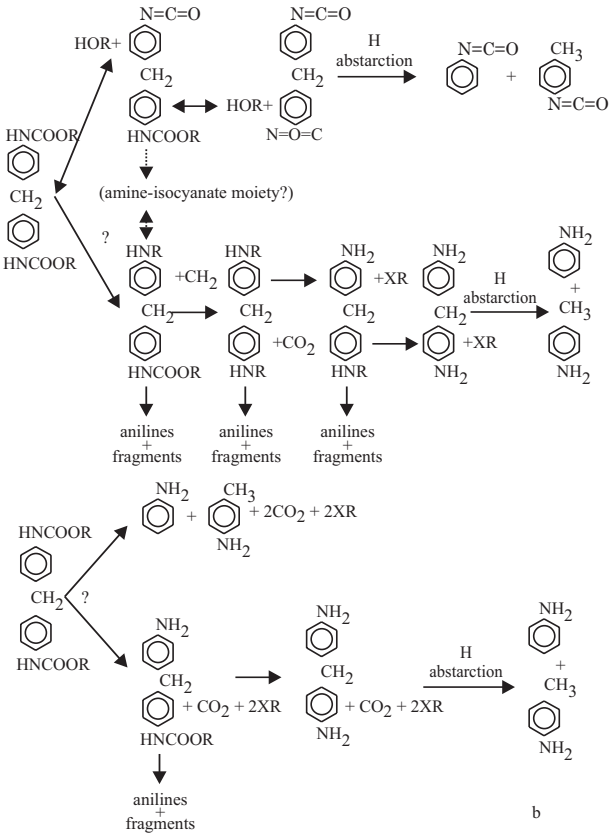

Fig. 11 MDI RPU decomposition reactions: a – isocyanate-polyamine and b – anilines from urethane moieties

and the competing reaction to evolve carbon dioxide and form an amine moiety is more prevalent. Furthermore, bond scission appears to occur at comparable rates at the methylene group between the aromatic rings in the MDI. This results in evolution of isocyanates, probably phenylisocyanates, as well as evolution of aniline and 4-methyl aniline from the amine moieties that form. The reactions forming the amine moieties appear similar to those occurring in TDI RPU. Figure 11 shows a set of reactions involving the urethane moiety in MDI RPU that appear consistent with the experimental data. Again, it is not clear if the anilines evolve from bond scission in a polyamine (Fig. 11a) or form directly from urethane moieties (Fig. 11b).

Epoxy

Figure 12 shows replicate TG results from samples of the epoxy that were heated at a constant rate of 15°C min^{-1}. Results for unconfined and partially-confined samples are shown. At temperatures below 300°C, the curves for partially-confined samples (Fig. 12) are shifted to much higher temperatures

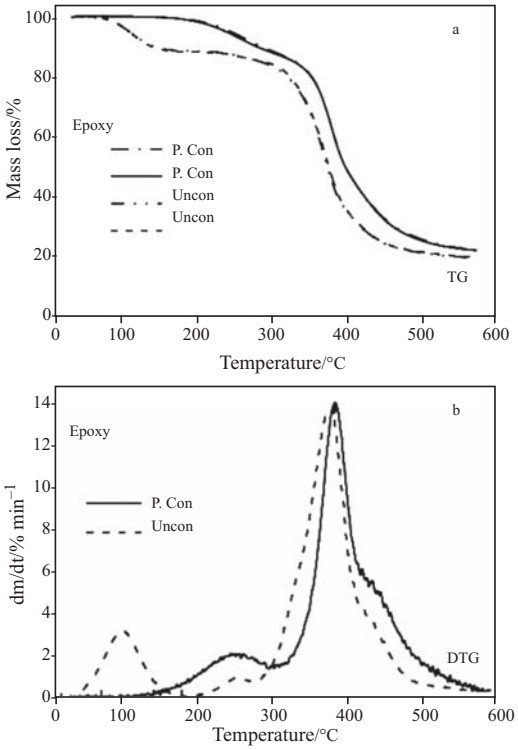

Fig. 12 Typical a – TG and b – DTG results for unconfined and partially-confined (60 μm orifice) samples of epoxy

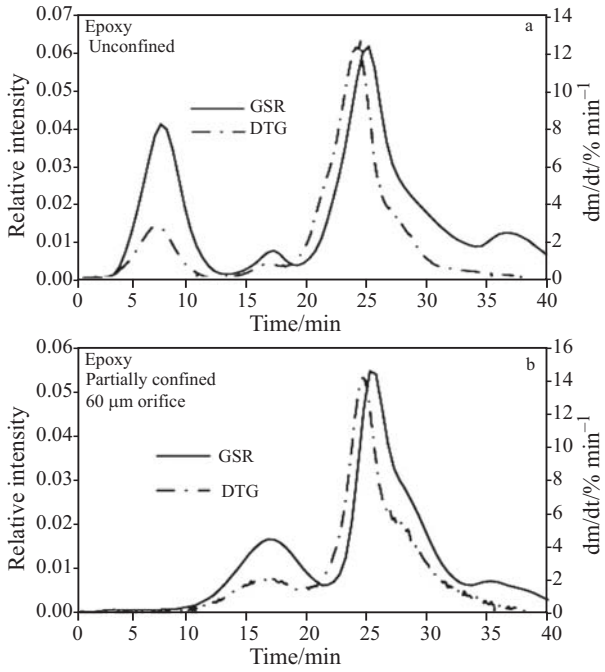

Fig. 13 Gramm-Schmidt reconstruction (GSR) for epoxy samples: a – unconfined and b – partially-confined

relative to the curves for unconfined samples. At temperatures above 300°C, the curves for partially-confined samples are still shifted, but only by about 25°C. In Fig. 12b, the derivative curve for the unconfined sample shows three peaks. The curve for the partially-confined sample shows two peaks, and the larger peak has a shoulder at higher temperatures.

Results from DSC experiments with unconfined samples showed a mild endothermic peak that closely corresponded to the small peak at about 120°C in the TG derivative curve in Fig. 12b. At temperatures between about 300 and 400°C, the heat flow to the sample significantly decreased, although the heat flow never became exothermic before becoming more endothermic at temperatures above 400°C. The sharp decrease in heat flow occurs over the temperature range in which the rate of mass loss is greatest and may indicate the presence of secondary reactions.

During the TG experiments, FTIR spectra were collected as described previously. Figure 13 shows the GSR from the FTIR spectra that were collected during the unconfined and partially-confined TG experiments shown in Fig. 12. For comparison, the rate-of-mass-loss data in Fig. 12b are shown as a function of time in Fig. 13. FTIR spectra corresponding to the peaks at about 7 and 25 min in the GSR for the unconfined sample shown in Fig. 13a are shown in Figs 14a and b, respectively. FTIR spectra corresponding to the peaks at about 16 and 25 min in the GSR for the partially-confined sample shown in Fig. 13b are shown in Figs 15a and b, respectively.

The spectra in Figs 14a and 15a are essentially identical, except for a difference in overall signal intensity. The spectra in Figs 14b and 15b are also essentially identical except for overall signal intensity. Although the TG curves for the partially-confined samples were shifted relative to the curves for the unconfined samples, the decomposition products that evolved did not appear to change significantly from unconfined to partially-confined samples. This indicates that major changes in the decomposition mechanism did not occur. This is particularly true in the temperature range from 300 to 500°C, in which most decomposition occurs. The FTIR spectra collected during the TG experiments indicated products containing phenol moieties, with spectra reasonably matching 4-t-butylphenol and bisphenol A. However, the decomposition products could not be clearly identified.

Experiments using the TDS-GC-FTIR system were done in two stages. In the first stage, the sample was heated at a rate of 20°C min^{-1} to 200°C, held at 200°C for 30 min, and then quenched. In the second stage, the sample was heated at a rate of 20°C min^{-1} to 340°C, held at 340°C for 30 min, and then quenched. The GSR from the first stage contained only one major peak. The corresponding spectrum matched the spectrum for 4-t-butylphenol. The GSR from the second stage of an experiment is shown in Figure 16a. Several decomposition products were identified from

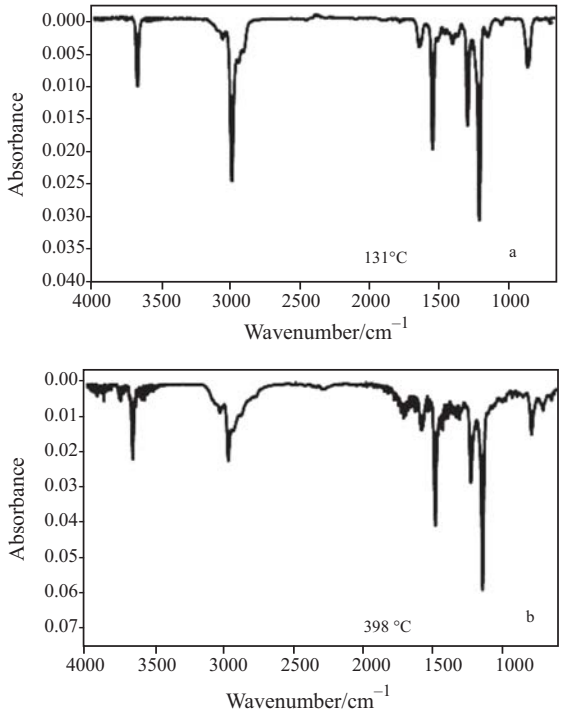

Fig. 14 Unconfined epoxy: FTIR spectra corresponding to GSR at a – 6.953 and b – 24.586 min

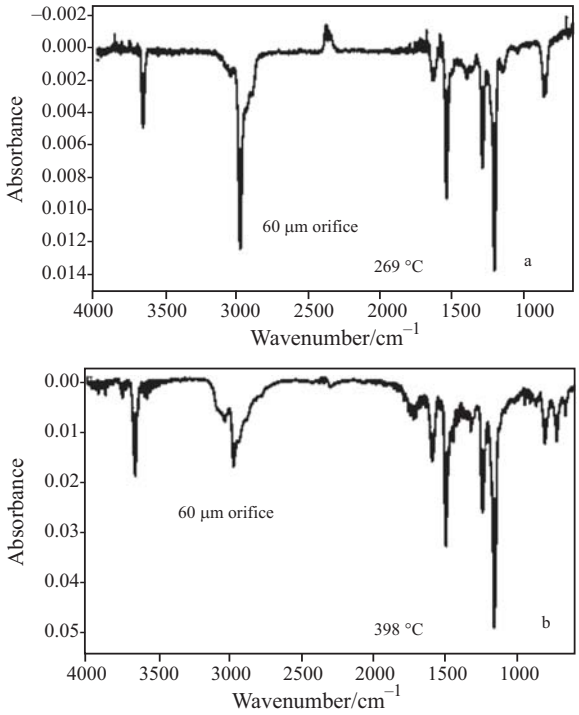

Fig. 15 Partially-confined epoxy: FTIR spectra corresponding to GSR at a – 16.021 and b – 24.586 min

a library search [69]. The broad peak between about 2 and 4 min is a mixture of water and carbon dioxide. The FTIR spectra from the major peaks at 10.496 min (shown in Fig. 16b), 13.978, 15.197 and 15.894 min matched the spectra for phenol, 4-isopropylphenol,

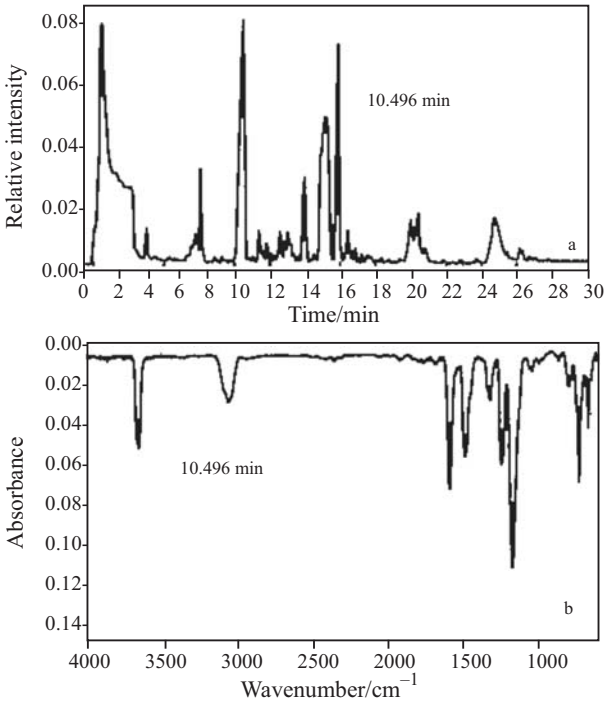

Fig. 16 Results from a TDS-GC-FTIR experiment with epoxy: a – GSR and b – sample spectrum

bisphenol A, and 4-t-butyl-*o*-cresol, respectively. The phenol, 4-isopropylphenol, and bisphenol A appear to evolve from the bisphenol A moiety in the polymer. The 4-t-butyl-*o*-cresol may be associated with the curing agent.

Evolution of phenol, 4-isopropylphenol, and bisphenol A from the epoxy indicate that bond scission involving the bisphenol A moiety in the epoxy is a major decomposition mechanism. Scission appears to occur with comparable rates at the isopropyl group between the aromatic rings and at the carbon-oxygen bond opposite to the aromatic rings. Figure 17 illustrates reactions involving the bisphenol A moiety that are consistent with the experimental data. Reactions involving other moieties also probably occur.

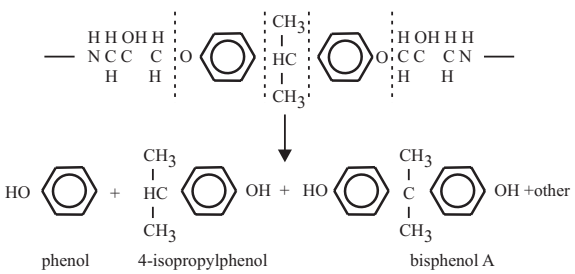

Fig. 17 Epoxy decomposition reactions involving the bisphenol A moiety in the polymer

Poly(diallyl phthalate) and polycarbonate

Thermal decomposition of unconfined samples of poly(diallyl phthalate), which contained inert filler, was examined using TG-FTIR, DSC, and TDS-GC-FTIR. The DSC results indicated an essentially endothermic decomposition process that corresponded to the rate of mass loss from TG experiments. The FTIR spectra from the TG experiments indicated that the major decomposition product was phthallic anhydride. Experiments done using the TDS-GC-FTIR system confirmed that phthallic anhydride was the major product, and also identified acetic acid, benzoic acid, and phthalide. The overall reaction that appears to dominate decomposition is shown in Fig. 18.

Initial results from TG experiments with unconfined polycarbonate (Lexan®) samples were included in Fig. 2, because previous reports [11] indicated decomposition mechanisms (Fig. 19) that are somewhat analogous to those described above.

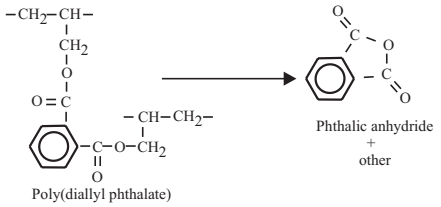

Fig. 18 Poly(diallyl phthalate) decomposition reactions involving phthalate moiety in the polymer

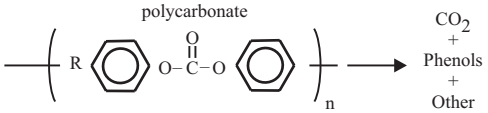

Fig. 19 Polycarbonate decomposition reactions involving aromatic carbonate moiety in the polymer

Poly(phenylene sulphide)

Thermal decomposition of unconfined samples of poly(phenylene sulphide) (Fortron®) was examined using TG-FTIR, DSC, and TDS-GC-FTIR. DSC results indicated an endothermic decomposition process that corresponded to the rate of mass loss from the TG experiments. The FTIR spectra collected during the TG experiments indicated that the major decomposition products were phenylene sulphides, but none were identified with certainty. Results from a TDS-GC-FTIR experiment are shown in Fig. 20.

The GSR from the TDS-GC-FTIR experiment is shown in Fig. 20a. The spectrum corresponding to the large peak at 10.247 min is shown in Fig. 20b. The spectrum in Fig. 20b matches the spectrum for benzenethiol [69]. Diphenyl disulphide and possibly

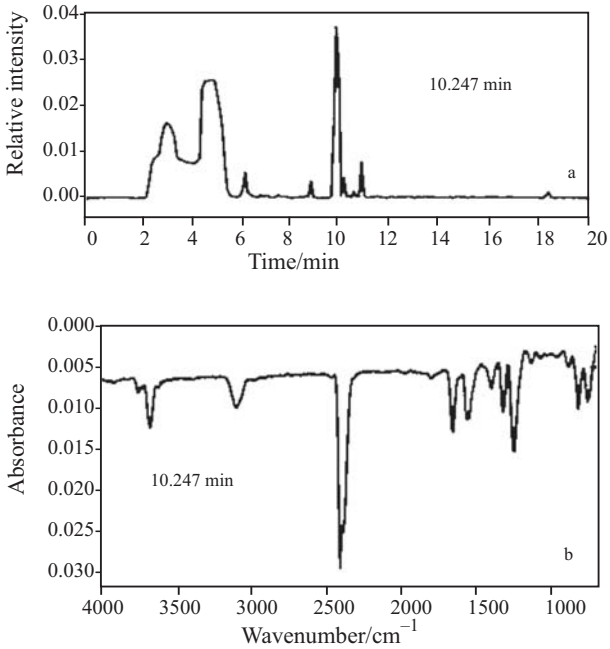

Fig. 20 Results of TDS-GC-FTIR experiment with poly(phenylene sulfide) (Fortron®): a – GSR and b – sample spectrum

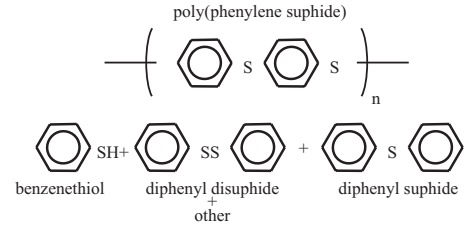

Fig. 21 Poly(phenylene sulphide) decomposition reactions

diphenyl sulphide also were identified. The decomposition process is represented in Fig. 21.

Conclusions

The experimental results indicate a consistent set of chain scission reactions involving the aromatic moieties in the materials studied. The common modes of bond scission are shown in Fig. 22. The rates of reaction depend on the atoms involved in scission, the rates of radical formation and recombination, the potential for hydrogen abstraction, and the potential for ring formation, such as formation of phthalic anhydride during decomposition of diallyl phthalate.

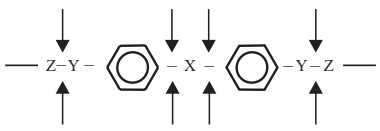

Fig. 22 Common modes of bond scission involving the aromatic moieties in the polymers studied

Acknowledgements

The author gratefully acknowledges the considerable technical assistance provided by John Oelfke and Ted Borek of Sandia National Laboratories.

References

1 Sandia is a multi-program laboratory operated by Sandia Corporation, a Lockheed Martin Company, for the United States Department of Energy's National Nuclear Security Administration under contract DE-AC04-94AL8500.
2 D. Drysdale, An Introduction to Fire Dynamics, 2nd Ed., John Wiley and Sons, Chichester 2002.
3 V. Babrauskas and S. J. Grayson, Heat Release in Fires, Chapman and Hall, London 1996.
4 G. L. Nelson and C. A. Wilkie (Eds), Fire and Polymers: Materials and Solutions for Hazard Prevention, ACS symposium Series, American Chemical Society, Washington D. C. 2001.
5 G. L. Nelson and C. A. Wilkie, (Eds) Fire and Polymers IV: Materials and Solutions for Hazard Prevention, ACS symposium Series, American Chemical Society, Washington D. C. 2006.
6 K. L. Erickson, S. M. Trujillo, K. R. Thompson, A. C. Sun, M. L. Hobbs and K. J. Dowding in Computational Methods in Materials Characterization, A. A. Mammoli and C. A. Brebbia, WIT Press, Southhampton UK 2004.
7 A. C. Sun, K. L. Erickson, M. L. Hobbs, D. Adolf and M. Stavig, Computational Methods in Materials Characterization, A. A. Mammoli and C. A. Brebbia, (Eds), WIT Press, Southhampton UK 2004.
8 M. L. Hobbs and G. H. Lemmon, Computational Methods in Materials Characterization, A. A. Mammoli and C. A. Brebbia, Eds, WIT Press, Southhampton, UK, (2004).
9 M. L. Hobbs, K. L. Erickson and T. Y. Chu, Polym. Degrad. Stab., 69 (2000) 47.
10 S. L. Madorsky, Thermal Degradation of Organic Polymers, Interscience Publishers, a division of John Wiley and Sons, New York 1964.
11 A. Ravve, Principles of Polymer Chemistry, 2nd Ed., Kluwer Academic/Plenum Publishers, New York 2000, pp. 581–616.
12 P. J. Haines, Ed., Principles of Thermal Analysis and Calorimetry, Royal Society of Chemistry, Cambridge 2002.
13 M. Sorai, Ed., Comprehensive Handbook of Calorimetry and Thermal Analysis, John Wiley and Sons, West Sussex, England 2004.
14 J. Šesták, Heat, Thermal Analysis and Society, Nucleus HK 2004.
15 V. F. Nicolette, K. L. Erickson and B. E. Vembe, in Proceedings of Interflam 2004, 10th International Conference on Fire Science and Engineering, Edinburgh, Scotland, July 5–7, 2004, Interscience Communications Ltd. London.
16 B. E. Vembe, V. F. Nicolette and K. L. Erickson, in Proceedings of International Technical Conference: Computational Simulation Models in Fire Engineering and Research, hosted by the University of Cantabria (Spain), October 2004.
17 H. Polli, L. A. M. Pontes, M. J. B. Souza, V. J. Fernandes Jr. and A. S. Araujo, J. Therm. Anal. Cal., 86 (2006) 469.
18 D. K. Dash, S. K. Sahu and P. L. Nayak, J. Therm. Anal. Cal., 86 (2006) 517.
19 M. Gao, C. Y. Sun and C. X. Wang, J. Therm. Anal. Cal., 85 (2006) 765.
20 V. Alvarez, E. Rodriguez and A. Vázquez, J. Therm. Anal. Cal., 85 (2006) 383.
21 K. Pielichowski and B. Świerz-Motysia, J. Therm. Anal. Cal., 83 (2006) 207.
22 R. López-Fonseca, I. Landa, M. A. Gutiérrez-Ortiz and J. R. González-Velasco, J. Therm. Anal. Cal., 80 (2005) 65.
23 K. Pielichowski and B. Janowski, J. Therm. Anal. Cal., 80 (2005) 147.
24 Z. Y. Ren, W. Y. Liu, Y. M. Hou, L. K. Zhu, L. K. Chang and D. Z. Ma, J. Therm. Anal. Cal., 63 (2001) 153.
25 I. M. M. Kenawy, M. A. H. Hafez and Kh. S. El-Said, J. Thermal Anal., 42 (1994) 1143.
26 A. M. L. Silva, R. W. Li, C. J. R. Matos and J. Gruber, J. Therm. Anal. Cal., 59 (2000) 675.
27 R. Kotsilkova, V. Petkova and Y. Pelovski, J. Therm. Anal. Cal., 64 (2001) 591.
28 A. F. Naves, P. M. Kosaka, J. R. Matos and D. F. S. Petri, J. Therm. Anal. Cal., 79 (2005) 389.
29 L. Šlusarski and G. Janowska, J. Thermal Anal., 19 (1980) 435.
30 G. Liptay, J. Nagy, J. Ch. Weis and A. Borbély-Kuszmann, J. Thermal Anal., 32 (1987) 1421.
31 H. Abematsu, M. Tsuchiya, Y. Iseri and T. Kojima, J. Therm. Anal. Cal., 56 (1999) 1093.
32 H. S. Kim, H. S. Yang, H. J. Kim and H. J. Park, J. Therm. Anal. Cal., 76 (2004) 395.
33 Y. N. Bolbukh, V. A. Tertykh and B. Gawdzik, J. Therm. Anal. Cal., 86 (2006) 125.
34 L. Núñez-Regueira, M. Villanueva and I. Fraga-Rivas, J. Therm. Anal. Cal., 83 (2006) 727.
35 L. Núñez and M. Villanueva, J. Therm. Anal. Cal., 80 (2005) 141.
36 B. Howell and J. Zhang, J. Therm. Anal. Cal., 83 (2006) 83.
37 D. Chambree, C. Idioiu, E. Segal and A. Cesáro, J. Therm. Anal. Cal., 82 (2005) 803.
38 H. Polli, L. A. M. Pontes and A. S. Araujo, J. Therm. Anal. Cal., 79 (2005) 383.
39 J. M. Criado, L. A. Pérez-Maqueda and P. E. Sánchez-Jiménez, J. Therm. Anal. Cal., 82 (2005) 671.
40 J. M. Criado and L. A. Pérez-Maqueda, J. Therm. Anal. Cal., 84 (2005) 453.
41 J. Rychlý, L. Matisová-Rychlá and M. Vavreková, J. Thermal Anal., 25 (1982) 423.
42 P. Budrugeac and E. Segal, J. Thermal Anal., 53 (1998) 269.
43 I. A. Schneider and A. Cs. Bíró, J. Thermal Anal., 5 (1973) 293.
44 X.-R. Li and H. Koseki, J. Therm. Anal. Cal., 85 (2006) 637.
45 A. Gröbler and T. Kada, J. Thermal Anal., 5 (1973) 407.
46 A. K. Galwey, J. Therm. Anal. Cal., 86 (2006) 267.
47 B. A. Howell, J. Therm. Anal. Cal., 85 (2006) 165.
48 B. A. Howell and J. A. Ray, J. Therm. Anal. Cal., 83 (2006) 63.
49 S. Vyazovkin, J. Therm. Anal. Cal., 83 (2006) 45.
50 M. E. Brown, J. Therm. Anal. Cal., 82 (2005) 665.

51 P. Šimon, J. Therm. Anal. Cal., 82 (2005) 651.
52 P. Šimon, J. Therm. Anal. Cal., 79 (2005) 703.
53 T. Ozawa, J. Therm. Anal. Cal., 82 (2005) 687.
54 T. Kojima, M. Tsuchiya, K. Ishimaru and T. Yamada, J. Therm. Anal. Cal., 80 (2005) 137.
55 R. Bigda and A. Mianowski, J. Therm. Anal. Cal., 84 (2005) 453.
56 O. F. Shlensky, J. Thermal Anal., 44 (1995) 1113.
57 O. F. Shlensky, L. N. Aksenov and A. G. Shashkov, Thermal Decomposition of Materials: Effect of Highly Intensive Heating, Elsevier, Amsterdam 1991.
58 P. Rybiński, G. Janowska, W. Antkowicz and S. Krauze, J. Therm. Anal. Cal., 81 (2005) 9.
59 J. Chruściel, G. Janowska, P. Rybiński and L. Ślusarski, J. Therm. Anal. Cal., 84 (2006) 344.
60 B. A. Howell, D. A Spears and P. B. Smith, J. Therm. Anal. Cal., 85 (2006) 115.
61 F. S. M. Sinfrônio, A. G. Souza, M. G. Santos Ieda, V. J. Fernandes Jr., Cs. Novák and Zs. Éhen, J. Therm. Anal. Cal., 85 (2006) 391.
62 A. Pappa, K. Mikedi, N. Tzamtzis and M. Statheropoulos, J. Therm. Anal. Cal., 84 (2006) 655.
63 K. Pielichowski, J. Therm. Anal. Cal., 54 (1998) 171.
64 K. Pielichowski and L. Stoch, J. Therm. Anal. Cal., 45 (1995) 407.
65 C. N. Caşcaval, N. Hurduc and Ig. C. Poinescu, J. Thermal Anal., 34 (1988) 311.
66 W. Xie and W.-P. Pan, J. Therm. Anal. Cal., 65 (2001) 669.
67 W. Xie, W.-P. Pan and K. C. Chuang, J. Therm. Anal. Cal., 64 (2001) 477.
68 T. Tsugoshi, T. Nagaoka, K. Hino. T. Arii, M. Inoue, Y. Shiokawa and K. Watari, J. Therm. Anal. Cal., 80 (2005) 787.
69 OMNIC software and Nicolet vapor phase FTIR library, Thermo-Electron Corp., Madison, Wisconsin.
70 K. L. Erickson, Proceedings of SAMPE 2006, Long Beach, Ca, April 30–May 5, 2005.

DOI: 10.1007/s10973-006-8218-6